

Hyperbolic Metric Learning for Visual Outlier Detection

Alvaro Gonzalez-Jimenez^{1,2} Simone Lionetti² Dena Bazazian³ Philippe Gottfrois¹

Fabian Gröger^{1,2} Marc Pouly² Alexander Navarini¹

¹University of Basel ²Lucerne University of Applied Sciences and Arts ³University of Plymouth

{alvaro.gonzalezjimenez, philippe.gottfrois, alexander.navarini}@unibas.ch

{simone.lionetti, fabian.groger, marc.pouly}@hslu.ch

dena.bazazian@plymouth.ac.uk

Abstract

Out-Of-Distribution (OOD) detection is critical to deploy deep learning models in safety-critical applications. However, the inherent hierarchical concept structure of visual data, which is instrumental to OOD detection, is often poorly captured by conventional methods based on Euclidean geometry. This work proposes a metric framework that leverages the strengths of Hyperbolic geometry for OOD detection. Inspired by previous works that refine the decision boundary for OOD data with synthetic outliers, we extend this method to Hyperbolic space. Interestingly, we find that synthetic outliers do not benefit OOD detection in Hyperbolic space as they do in Euclidean space. Furthermore we explore the relationship between OOD detection performance and Hyperbolic embedding dimension, addressing practical concerns in resource-constrained environments. Extensive experiments show that our framework improves the FPR95 for OOD detection from 22% to 15% and from 49% to 28% on CIFAR-10 and CIFAR-100 respectively compared to Euclidean methods.

1. Introduction

The field of Deep Learning (DL) has witnessed remarkable advancements, revolutionizing various domains from image recognition to natural language processing. While these models excel within their training data distribution, a critical challenge arises when encountering unforeseen data. This can lead to overly confident predictions with potentially disastrous real-world consequences.

Out-Of-Distribution (OOD) detection has emerged as a pivotal research area aimed at addressing this challenge. Its objective is the identification of inputs that deviate significantly from the training data distribution, thereby enabling the safe deployment of DL models in scenarios where encountering novel or unexpected data is inevitable such as

medical imaging and autonomous vehicles, where erroneous predictions can have life-threatening implications.

Existing OOD detection approaches suffer from overconfidence on OOD data with higher likelihood leading to unreliable uncertainty estimates [58], rely on the quality of feature embeddings [54, 66] or require the use of external auxiliary OOD data [5, 20, 25, 32, 50, 51, 74], which poses challenges especially when the exact nature of the OOD data is unknown. Synthesizing outliers from the low-likelihood feature space of ID data has emerged as an alternative to obtain this auxiliary data [16, 67]. However, this assumes that OOD samples lie on the periphery of the ID distribution, which may not always be true. As a result, synthesized outliers may not accurately reflect the characteristics of true OOD data, leading to suboptimal detection performance.

One common ingredient that all the previously mentioned frameworks share is that they are based on *Euclidean* geometry. In this paper, we argue that real-world visual data often exhibit intricate hierarchical structures, such as the organization of diseases in medical imaging. However, Euclidean geometry fails to accurately capture these hierarchical relationships, leading to suboptimal representations [7]. Herein lies our motivation for exploring *Hyperbolic* geometry as an alternative.

In Hyperbolic geometry, unlike in Euclidean geometry, two parallel lines can pass through a distinct point. This distinction defines Hyperbolic space as a framework of constant negative curvature, known for its hierarchical organization and exponential expansion properties [7]. Recent interest in Hyperbolic space for Computer Vision (CV) has spurred significant advancements in embedding complex hierarchical structures with minimal distortion [63, 65]. This offers distinct advantages across various domains, including few-shot learning [35, 61], unsupervised learning [60], and representation learning [14, 19, 40]. Moreover, previous research hints at the potential of Hyperbolic space for OOD detection, leveraging uncertainty measurements

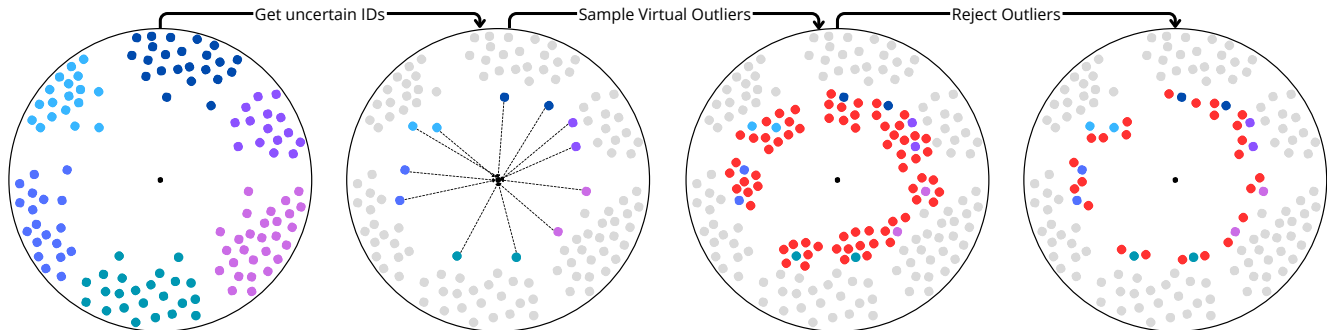


Figure 1. Illustration of the Hyperbolic outliers synthesis. First, the In-Distribution (ID) embeddings are optimized using Eq. (7) which encourages low intra-class variation and inter-class separation. Second, the most uncertain ID embeddings are selected by their distance towards the origin. Third the outliers are synthesized by sampling from the wrapped Gaussian distribution centered around the selected ID embeddings. Finally, only those with a higher level of certainty are kept.

based on the distance of the embeddings from the origin in the Poincaré disk [2, 35] or using the energy-based score [23, 69]. However, the model performance is yet not competitive with the Euclidean-based models.

We hypothesize that the gap between Euclidean and Hyperbolic space arises from differences in the training objectives employed, particularly concerning *intra-class* variation and *inter-class* separation. Intra-class variation evaluates the consistency of representations across diverse environments, whereas inter-class separation gauges the spread of characteristics across distinct classes. Ideally, features should exhibit minimal variation within classes and significant separation between classes to effectively detect OOD data.

Thus in this paper, we propose HOD (**H**yperbolic **O**utlier **D**etection) a framework that leverages the Hyperbolic space to learn ID representations promoting low variations and high separation. Our learning objective establishes a new state-of-the-art in OOD detection, with an improvement in the FPR95 from 22% to 15% and from 49% to 28% on CIFAR-10 and CIFAR-100 respectively compared to current Euclidean methods. Through empirical evaluations, we demonstrate the effectiveness of certain techniques to detect OOD in the Hyperbolic space while identifying others that are not suitable. Furthermore, we propose the first strategy for synthesizing outliers in the Hyperbolic space that works on par with the metric objective. We demonstrate that Hyperbolic space is better suited for deployment in real-world scenarios, particularly in resource-constrained environments requiring low-dimensional embeddings. This opens doors for practical applications in various industrial domains.

2. Preliminaries

We consider a training set $D = \{(\mathbf{x}_i, y_i)\}_{i=1}^N$, drawn *i.i.d.* from the joint data distribution $\mathcal{P}_{\mathcal{X}\mathcal{Y}}$, where \mathcal{X} denotes the

input space and $\mathcal{Y} \in \{1, 2, \dots, \mathcal{C}\}$ denotes the label space with \mathcal{C} the number of classes. Let \mathbb{P}_{id} be the marginal distribution on \mathcal{X} , which is also referred to as the *in-distribution*.

2.1. Out-of-Distribution Detection

Out-Of-Distribution detection can be conceptualized as a task of distinguishing between two classes. During testing, the objective of OOD detection is to determine whether a given sample $x \in \mathcal{X}$ originates from \mathbb{P}_{id} or is out-of-distribution. This task can be addressed by integrating a novelty detection mechanism during deployment that detects samples deviating from the known distribution, such as samples from an unrelated distribution with a label set disjoint from the in-distribution \mathcal{Y}_{id} , and thus should not be predicted by the model. Formally, let $D_{\text{ood}}^{\text{test}}$ represent an out-of-distribution test set where the label space $\mathcal{Y}_{\text{ood}} \cap \mathcal{Y}_{\text{id}} = \emptyset$. The decision can be made employing level set estimation: $\mathcal{G}_\lambda(x) = 1 \{S(x) \geq \lambda\}$, where samples with higher scores $S(x)$ are classified as ID, and vice versa. The threshold λ is typically selected such that a substantial portion of in-distribution data *e.g.* 95% is accurately classified.

2.2. Hyperbolic Space

Hyperbolic geometry is a non-Euclidean geometry characterized by constant negative curvature. It diverges from Euclidean geometry by permitting infinitely many parallel lines to intersect a given line. Various models, such as the Poincaré disk, Poincaré half-plane, Beltrami–Klein, and Lorentz (Hyperboloid/Minkowski) models, have been employed to depict Hyperbolic space [41, 52]. Although the Poincaré disk has been widely used in the research community [59, 68, 69] this study adopts the Lorentz model due to its simpler closed-form representation of geodesics [14, 40] and its robustness to numerical instabilities, as discussed in [55]. Given the $n + 1$ -dimensional Minkowski space, represented by the vector $\mathbf{z} = [z_{\text{time}}, z_{\text{space}}] \in \mathbb{R}^{n+1}$ with the

Lorentz product

$$\langle \mathbf{z}, \mathbf{z}' \rangle_{\mathbb{L}} = \langle z_{\text{space}}, z'_{\text{space}} \rangle - z_{\text{time}} z'_{\text{time}} \quad (1)$$

the Lorentz model \mathbb{L}_c^n of an n -dimensional Hyperbolic space with curvature c is the manifold defined by $\langle \mathbf{z}, \mathbf{z}' \rangle_{\mathbb{L}} = -1/c$ with $z_{\text{time}} = \sqrt{1/c + \|z_{\text{space}}\|}$. In this context, the Lorentzian norm is given by $\|\mathbf{z}\|_{\mathbb{L}} = \sqrt{\langle \mathbf{z}, \mathbf{z} \rangle_{\mathbb{L}}}$.

Definition 2.1 (Geodesic). A geodesic is the shortest path between two points on a curved surface or manifold, analogous to a straight line in Euclidean space. The *Lorentz distance* between two points $\mathbf{x}, \mathbf{y} \in \mathbb{L}_c^n$ is:

$$d_{\mathbb{L}}(\mathbf{x}, \mathbf{y}) = \sqrt{\frac{1}{c}} \cdot \cosh^{-1}(-c \langle \mathbf{x}, \mathbf{y} \rangle_{\mathbb{L}}) \quad (2)$$

Definition 2.2 (Tangent space). The tangent space at some point $\mathbf{z} \in \mathbb{L}_c^n$ is a Euclidean space of vectors orthogonal to \mathbf{z} according to the Lorentz product:

$$\mathcal{T}_{\mathbf{z}} \mathbb{L}_c^n = \{ \mathbf{v} \in \mathbb{R}^{n+1} : \langle \mathbf{z}, \mathbf{v} \rangle_{\mathbb{L}} = 0 \} \quad (3)$$

Any vector $\mathbf{u} \in \mathbb{R}^{n+1}$ can be projected to the tangent space $\mathcal{T}_{\mathbf{z}} \in \mathbb{L}_c^n$ via orthogonal projection:

$$\mathbf{v} = \text{proj}_{\mathbf{z}}(\mathbf{u}) = \mathbf{u} + c\mathbf{z} \langle \mathbf{z}, \mathbf{u} \rangle_{\mathbb{L}} \quad (4)$$

Definition 2.3 (Exponential and Logarithmic maps). The *exponential map* provides a way to map a vector from the tangent spaces onto the manifold. Formally, for a point \mathbf{z} on the hyperboloid, it is defined as $\text{exp}_{\mathbf{z}} : \mathcal{T}_{\mathbf{z}} \mathbb{L}_c^n \rightarrow \mathbb{L}_c^n$ with the expression:

$$\mathbf{x} = \text{exp}_{\mathbf{z}}(\mathbf{v}) = \cosh(\sqrt{c}\|\mathbf{v}\|_{\mathbb{L}})\mathbf{z} + \frac{\sinh(\sqrt{c}\|\mathbf{v}\|_{\mathbb{L}})}{\sqrt{c}\|\mathbf{v}\|_{\mathbb{L}}}\mathbf{v} \quad (5)$$

The inverse operation is the *logarithmic map* $\text{log}_{\mathbf{z}} \mathbb{L}_c^n \rightarrow \mathcal{T}_{\mathbf{z}} \mathbb{L}_c^n$ that maps \mathbf{x} from the Lorentz manifold \mathbb{L}_c^n back to \mathbf{v} in the tangent space:

$$\mathbf{v} = \text{log}_{\mathbf{z}}(\mathbf{x}) = \frac{\cosh^{-1}(-c \langle \mathbf{z}, \mathbf{x} \rangle_{\mathbb{L}})}{\sqrt{c \langle \mathbf{z}, \mathbf{x} \rangle_{\mathbb{L}}^2 - 1}} \quad (6)$$

For our approach we will consider these maps where in \mathbf{z} is the origin of the hyperboloid ($\mathbf{O} = [\mathbf{0}, \sqrt{\frac{1}{c}}]$).

3. Hyperbolic Space for Out-of-Distribution Detection

3.1. Compact Representation of In-Distribution Embeddings

Our objective is to leverage the properties of Hyperbolic space to improve the effectiveness of learned embeddings

in distinguishing between ID and OOD data. To achieve this, we use a feature encoder $f_{\theta} : \mathcal{X} \rightarrow \mathbb{R}^e$ that transforms the augmented input $\mathbf{x} \in \mathcal{X}$ into a high-dimensional image embedding $f_{\theta}(\mathbf{x})$, often referred to as penultimate layer features.

Since these embeddings reside in Euclidean space, we need to project them onto the hyperboloid \mathbb{L}_c^n to operate within the Hyperbolic space. We accomplish this by applying the exponential map, as defined in Eq. (5). Following the approach proposed by [14], we focus solely on the *space* component of the *exponential map* to reduce computational complexity and eliminate the orthogonal projection.

Once the embeddings are lifted into the Hyperbolic space, our next step involves optimizing them to encourage clustering embeddings belonging to the same class are pulled together, while simultaneously pushing apart clusters of samples from different classes. This optimization strategy follows a supervised contrastive learning approach [34] promoting low intra-class variation and high inter-class separation, but rather than relying on cosine similarity as in the Euclidean space, we compute the negative Lorentzian distance Eq. (2) as a similarity measure. The process solely involves training the parameters θ of the image feature encoder and the projection layer. It is guided by the loss function:

$$\mathcal{L}_{\text{hsup}} = \sum_{i \in I} \frac{-1}{|P(i)|} \sum_{p \in P(i)} \log \frac{\exp(-d_{\mathbb{L}}(\mathbf{z}_i, \mathbf{z}_p)/\tau)}{\sum_{a \in A(i)} \exp(-d_{\mathbb{L}}(\mathbf{z}_i, \mathbf{z}_a)/\tau)} \quad (7)$$

Here, $P(i) = \{p \in A(i) : \tilde{\mathbf{y}}_p = \tilde{\mathbf{y}}_i\}$ is the set of indices of all positives in the multiviewed batch distinct from i , and $|P(i)|$ is its cardinality.

As illustrated in Fig. 2, this function effectively improves the formation of tight clusters on the manifold while compelling in-distribution embeddings move towards the boundary. This characteristic also observed in prior research [2, 35], demonstrates that broader concepts in the hierarchy tend to cluster closer to the origin, while finer, more specific concepts are pushed towards the boundary. Leveraging this feature proves advantageous for both the classification of ID embeddings (discussed in Sec. 3.2) and the generation of new embeddings (explored in Sec. 3.3).

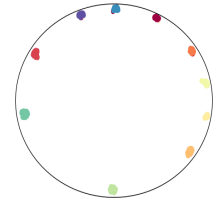


Figure 2. UMAP visualization of learned feature embeddings projected to the Poincaré disk using $\mathcal{L}_{\text{hsup}}$.

3.2. Classification of In-Distribution Embeddings

Traditional multi-class classification often relies on methods like Multinomial Logistic Regression (MLR). However, in our Hyperbolic setup, constructing a classifier involves determining the distance to margin hyperplanes within the Lorentz model. In this context, for a point $\mathbf{p} \in \mathbb{L}_c^n$ and a vector $\mathbf{w} \in \mathcal{T}_{\mathbf{p}}\mathbb{L}_c^n$, the hyperplane passing through \mathbf{p} and perpendicular to \mathbf{w} is represented by:

$$H_{\mathbf{w},\mathbf{p}} = \{\mathbf{z} \in \mathbb{L}_c^n \mid \langle \mathbf{w}, \mathbf{z} \rangle_{\mathbb{L}} = 0\} \quad (8)$$

To address the non-convex optimization condition $\langle \mathbf{w}, \mathbf{w} \rangle_{\mathbb{L}} > 0$, a Euclidean reparametrization was introduced [44]. Further defined the Lorentz hyperplane as:

$$\tilde{H}_{\mathbf{o},a} = \{\mathbf{z} \in \mathbb{L}_c^n \mid \cosh(\sqrt{c}a) \langle \mathbf{o}, z_{\text{space}} \rangle - \sinh(\sqrt{c}a) \|\mathbf{o}\| z_{\text{time}} = 0\} \quad (9)$$

Here, a represents the distance to the origin, and \mathbf{o} indicates the orientation. Finally, we need the distance to the hyperplane to quantify the model’s confidence [44]:

$$d_{\mathbb{L}}(\mathbf{z}, \tilde{H}_{\mathbf{o},a}) = \frac{1}{\sqrt{c}} \left| \sinh^{-1} \left(\sqrt{c} \frac{\cosh(\sqrt{c}a) \langle \mathbf{o}, z_{\text{space}} \rangle - \sinh(\sqrt{c}a) \|\mathbf{o}\| z_{\text{time}}}{\sqrt{\|\cosh(\sqrt{c}a)\mathbf{o}\|^2 - (\sinh(\sqrt{c}a)\|\mathbf{o}\|)^2}} \right) \right| \quad (10)$$

Leveraging the inherent clustering of similar embeddings due to the Hyperbolic contrastive loss Eq. (7), the model constructs an effective hyperplane for robust class discrimination.

3.3. Regularization with Synthetic Hyperbolic Outliers

The absence of explicit knowledge regarding unknown inputs during training leads to challenges. Models, usually optimized solely on ID data, may produce decision boundaries beneficial for tasks like classification as seen previously but unsuitable for OOD detection. Incorporating external information from these unknowns through $D_{\text{ood}}^{\text{aux}}$ during training helps in assigning lower scores to randomly selected outliers, thereby establishing a clear boundary between ID and OOD samples. These chosen outliers should not only be diverse but also informative, resembling ID samples closely.

Building upon previous research that utilized synthetic outliers sampled in the feature space [16, 67], we propose a regularization approach for the model employing the Hyperbolic space, *i.e.* Hyperbolic synthetic outliers. Our central concept leverages the observation that broader concepts in the visual hierarchy are closer to the origin, allowing us to sample from them and enhance the compactness of the ID representation.

Specifically, let $\mathcal{Z} = \{\mathbf{z}_1, \mathbf{z}_2, \dots, \mathbf{z}_n\}$ denote the set of ID embeddings from the training data, where $\mathbf{z}_i \in \mathbb{L}_c^n$

represents a feature in the Hyperbolic space. For any embedding $\mathbf{z}_i \in \mathcal{Z}$, we compute its L_2 norm with respect to the origin. If an embedding has a small L_2 norm, it is likely to be uncertain. Therefore, we select embeddings with the smallest L_2 distances. Once we have identified a set of ambiguous ID embeddings, we synthesize outliers by sampling from a Hyperbolic wrapped Gaussian distribution [56] centered around the selected uncertain ID embedding $\mathbf{s} \sim \mathcal{WG}(\mathbf{z}_i, \sigma^2 \mathbf{I})$ where the $\mathbf{s} \in \mathbb{L}_c^n$ denotes the synthesized outlier around \mathbf{z}_i , and σ^2 modulates the variance. For each uncertain ID embedding we produce a set of synthetic outliers $\mathcal{S} = \{\mathbf{s}_1, \mathbf{s}_2, \dots, \mathbf{s}_n\}$.

Then, we further filter the synthetic outliers \mathbf{s}_j by selecting those with the highest L_2 distance (indicating higher certainty), but less than the ID embedding \mathbf{z}_i from which it originated $\|\mathbf{s}_j - \mathbf{z}_i\|_2 < \|\mathbf{z}_i\|_2$. The overall procedure can be visualized in Fig. 1.

The final collection of accepted synthetic outliers will be used for the binary training objective:

$$\mathcal{L}_{\text{uncertainty}} = \mathbb{E}_{\mathbf{v} \sim \mathcal{V}} \left[-\log \frac{1}{1 + \exp^{\tilde{H}_{\mathbf{o},a}(\mathbf{v})}} \right] + \mathbb{E}_{\mathbf{x} \sim \mathbb{P}_{\text{in}}} \left[-\log \frac{\exp^{\tilde{H}_{\mathbf{o},a}(\mathbf{x})}}{1 + \exp^{\tilde{H}_{\mathbf{o},a}(\mathbf{x})}} \right] \quad (11)$$

The loss function takes both the ID and synthesized outlier embeddings and aims to estimate a hyperplane $H_{\mathbf{o},a}(\cdot)$ that divides them through the binary cross-entropy loss. The final objective is formulated as a combination of the metric loss in Eq. (7) and the regularization loss Eq. (11) with a weighting factor α :

$$\mathcal{L} = \mathcal{L}_{\text{hsup}} + \alpha \mathcal{L}_{\text{uncertainty}} \quad (12)$$

By varying α , the relative importance of the synthetic outliers can be controlled, enabling flexibility in the optimization process.

4. Experimental Results

4.1. Setup

Datasets. Following common benchmarks in the literature, we consider CIFAR-10 [37], CIFAR-100 [37], and ImageNet-200 [12] as our in-distribution dataset D_{id} . We refrain from tuning hyperparameters specifically for each $D_{\text{ood}}^{\text{test}}$ dataset, thereby maintaining its unknown nature, akin to real-world scenarios. Subsequently, our considered validation out-of-distribution $D_{\text{ood}}^{\text{val}}$ datasets include LSUN [75], LSUN Resize [75], and iSUN [73]. For $D_{\text{ood}}^{\text{test}}$, we employ a suite of natural image datasets following the OpenOOD framework [76], which comprises SVHN [57], Places365 [77], Textures [10], and MNIST [13] for experiments involving CIFAR-10 and CIFAR-100. For experiments involving ImageNet-200, we utilize SSB [70], Ninco [6] as Near-OOD datasets, and iNaturalist [29], Textures [10] and OpenImage-O [71] as Far-OOD datasets.

Out-of-Distribution detection scores. They are determined using a distance-based approach during testing. An input $\mathbf{z} \in \mathbb{L}_c^n$ is classified as OOD if it exhibits significant distance from the ID data within the Hyperbolic embedding space. Our default method involves employing a straightforward non-parametric K-Nearest Neighbors (KNN) distance metric in the Hyperbolic space, which avoids imposing any distributional assumptions on the space and uses the potential of the exponential growth in the Hyperbolic space. Here, the distance is the negative Lorentzian distance Eq. (2) with respect to the k-th nearest neighbor.

Training details. In our primary experiments, we utilize ResNet-18 [24] as the backbone for all our experiments. We set the embedding dimension to 128 for the Hyperbolic projection head. To optimize the network, we employ AdamW [48] with a weight decay of 0.2 and $(\beta_1, \beta_2) = (0.9, 0.98)$. Weight decay is disabled for gains, biases, and learnable scalars *i.e.* curvature c . The training process spans 20K iterations with a batch size of 256 for CIFAR datasets and 512 for ImageNet-200. The maximum learning rate initiates at 1×10^{-3} , linearly increasing for the initial 400 iterations, followed by cosine decay to zero [47]. We set the weight of synthetic outliers as $\alpha = 0.1$ and commence sampling after 1,000 iterations.

Evaluation metrics. We report the following metrics: (1) the False Positive Rate (FPR95) of OOD samples when the true positive rate of ID samples is at 95% and (2) the Area Under the Receiver Operating Characteristic Curve (AUROC). Our evaluation consists of 3 independent training runs for all D_{id} . We average scores for the same random seed across datasets and report the mean and standard deviation for the seed. We further evaluated the statistical significance of observed differences by comparing our method to the best-performing baseline on each dataset and metric using a T-test, assuming statistical significance for p -values of less than $p = 0.05$ and denote this with **Bold**.

4.2. Evaluation on Hyperbolic Out-of-Distribution Scores

This section evaluates the effectiveness of different OOD detection scores. We compare three established methods previously used in the Hyperbolic space: Energy-score (EBO) [69], Softmax score [23] and the Distance to the origin [2, 35]. To select the best OOD detection strategy, we evaluate the models using the D_{out}^{val} metric while keeping the D_{out}^{test} undisclosed. We follow the procedure outlined in Sec. 4.1 but with a cross-entropy loss as the training objective. Subsequently, we evaluate the proposed \mathcal{L}_{hsup} Eq. (7) by pre-training the model and fine-tuning only the classification head.

The results, presented in Tab. 1, demonstrate that our detection score based on the Hyperbolic KNN outperforms the baselines with and without sampling synthetic outliers. Interestingly, pre-training the network with the \mathcal{L}_{hsup} reduces the FPR95 for some OOD detection scores. However, it does not provide any additional benefit for non-distance-based methods.

4.3. Main Results

Our comparison includes recent competitive approaches such as Energy score [46], ODIN score [30], MLS [28], GradNorm [31], ViM score [71], KNN distance [66], VOS [16], which synthesizes outliers by modeling ID embeddings as a mixture of Gaussian distribution and sampling from the low-likelihood region of the feature space, and NPOS [67], which samples outliers using a non-parametric approach. To ensure a fair and thorough comparison of the baseline models, we utilize the OpenOOD benchmark tool [76].

HOD outperforms Euclidean space methods. Our evaluation demonstrates superiority of the Hyperbolic space over traditional Euclidean methods in OOD detection tasks. In CIFAR-10 (see Tab. 2), HOD reduces the FPR95 from 22.47% using NPOS to 15.59%. Similarly, in CIFAR-100 (see Tab. 3), the reduction is even more substantial, decreasing from 52.52% to 28.98%. Notably, this improvement surpasses state-of-the-art methods by a substantial margin, with statistical tests supporting this claim. Figure 3 compares the Hyperbolic KNN scores between ID and OOD data. The ID scores cluster significantly higher, indicating closer distances to the reference points compared to the OOD distribution. This clear distinction in Hyperbolic KNN scores makes them effective for differentiating ID and OOD data, leading to more efficient OOD detection.

However, the results on the ImageNet-200 dataset are nuanced (see Tab. 4). While the margin between HOD and Euclidean approaches is not as large, our method still improves FPR95 in Near-OOD datasets SBB and Ninco and a large improvement for the Far-OOD OpenImages-O. This suggests that the advantage of Hyperbolic space might be dataset-dependent and potentially more pronounced in scenarios with less number of classes.

Synthetic outliers do not bring any benefit in Hyperbolic space. Our experiments demonstrate that incorporating synthetic outliers does not provide additional benefits for OOD detection using HOD. While such improvements were observed in Euclidean space with baselines like VOS [16] and NPOS [67], our findings suggest that the inherent properties of Hyperbolic space are sufficient for superior performance. We hypothesize that the limitations of the Hyperbolic Wrapped Gaussian might hinder its ability

Table 1. OOD detection performance on CIFAR-10 as D_{id} . The values are the mean and standard deviation after training each method three times on ResNet-18. **Bold** if there is a statistical significance difference.

Methods	D_{out}^{val}							
	LSUN		LSUN Resize		iSUN		Average	
	FPR95↓	AUROC↑	FPR95↓	AUROC↑	FPR95↓	AUROC↑	FPR95↓	AUROC↑
EBO	39.1±1.8	95.2±0.2	29.6±6.1	95.0±1.1	28.6±6.1	95.3±1.1	32.4±5.4	95.2±0.1
Softmax	17.6±1.8	96.9±0.2	31.6±7.0	94.9±1.2	30.3±7.1	95.1±1.2	26.5±7.7	95.6±1.1
Distance Origin	57.2±3.9	90.0±1.3	86.9±7.6	79.3±4.5	86.0±8.6	79.4±4.9	76.7±16.9	82.9±6.1
\mathcal{L}_{hsup} + EBO	32.4±5.6	95.2±0.9	57.7±0.4	88.1±0.2	61.8±2.8	87.4±1.0	50.6±15.9	90.2±4.3
\mathcal{L}_{hsup} + Softmax	9.3±0.5	97.9±0.1	41.6±0.5	90.8±2.5	46.0±0.7	91.5±0.0	32.3±20.0	93.4±3.9
\mathcal{L}_{hsup} + Distance Origin	10.3±0.1	97.6±0.1	62.0±0.8	87.3±0.1	66.1±1.1	86.5±0.2	46.1±31.1	90.5±6.2
HOD ($\alpha = 0$)	9.9±2.7	98.4±0.4	8.9±5.8	98.8±0.4	5.9±5.1	98.7±0.6	8.2±2.1	98.6±0.2
HOD ($\alpha = 0.1$)	10.3±0.6	97.2±0.6	2.7±1.7	99.3±0.2	1.8±0.2	99.4±0.0	4.9±4.6	98.6±1.2

Table 2. OOD detection performance on CIFAR-10 as D_{id} . The values are the mean and standard deviation after training each method three times on ResNet-18. **Bold** if there is a statistical significance difference.

Methods	D_{out}^{test}									
	Texture		Places365		SVHN		MNIST		Average	
	FPR95↓	AUROC↑	FPR95↓	AUROC↑	FPR95↓	AUROC↑	FPR95↓	AUROC↑	FPR95↓	AUROC↑
EBO [46]	51.8±7.5	89.5±0.9	54.5±8.0	89.3±1.0	35.1±7.5	91.8±1.2	25.0±15.8	93.0±2.6	41.7±6.5	90.9±1.0
ODIN [30]	67.7±13.6	86.9±2.8	70.3±8.5	85.1±1.5	68.6±0.6	84.6±1.0	23.8±15.1	95.2±2.4	57.6±5.2	88.0±0.8
MLS [28]	51.7±7.5	89.4±0.9	54.8±8.0	89.1±0.9	35.1±7.5	91.7±1.2	25.2±15.9	94.2±3.0	41.7±6.5	91.1±1.1
GradNorm [31]	98.1±0.6	52.1±5.0	92.5±2.8	60.5±6.5	91.7±3.0	53.9±7.8	85.4±6.0	63.7±9.0	91.9±2.7	57.5±3.9
ViM [71]	21.1±2.2	95.2±0.4	41.4±2.6	89.5±0.5	19.3±0.5	94.5±0.6	19.3±1.1	94.8±0.5	25.3±0.6	93.5±0.3
KNN [66]	24.1±0.7	93.2±0.3	30.4±0.8	91.8±0.3	22.6±1.6	92.7±0.4	20.1±1.7	94.3±0.5	24.3±0.5	93.0±0.2
VOS [16]	48.6±4.2	89.8±0.8	56.4±1.2	89.2±0.3	32.2±7.6	92.1±1.6	20.0±1.5	94.9±0.4	39.3±3.4	91.5±0.7
NPOS [67]	26.8±1.6	91.9±1.0	31.2±3.0	91.4±0.7	8.2±3.3	98.5±0.5	23.7±2.2	93.4±1.6	22.5±2.1	93.8±0.8
HOD ($\alpha = 0$)	19.3±2.0	97.8±0.1	10.6±0.3	98.4±0.4	12.4±0.4	98.0±0.4	21.1±6.3	96.8±1.5	15.8±1.2	97.8±0.4
HOD ($\alpha = 0.1$)	16.1±0.6	97.3±0.6	10.3±0.2	98.7±0.4	16.2±0.2	93.2±0.6	19.7±0.2	94.0±0.8	15.6±0.2	95.3±0.3

Table 3. OOD detection performance on CIFAR-100 as D_{id} . The values are the mean and standard deviation after training each method three times on ResNet-18. **Bold** if there is statistical significance difference.

Methods	D_{out}^{test}									
	Texture		Places365		SVHN		MNIST		Average	
	FPR95↓	AUROC↑	FPR95↓	AUROC↑	FPR95↓	AUROC↑	FPR95↓	AUROC↑	FPR95↓	AUROC↑
EBO [46]	62.4±2.5	78.4±1.0	58.7±1.0	79.2±0.3	53.8±3.8	82.0±2.2	53.7±5.4	79.6±1.4	57.1±2.5	79.8±0.8
ODIN [30]	62.4±3.6	79.3±1.3	60.5±0.7	79.1±0.3	67.4±4.8	74.7±0.9	44.6±3.4	84.4±1.4	58.7±1.0	79.4±0.3
MLS [28]	62.4±2.7	78.4±1.0	58.8±1.1	79.4±0.3	53.8±4.0	81.9±1.9	51.5±3.9	79.6±1.6	56.6±1.6	79.8±0.7
GradNorm [31]	92.4±0.7	64.6±0.2	84.6±1.0	69.5±1.0	69.2±10.6	73.6±9.2	85.6±1.9	66.1±1.2	82.9±2.7	68.4±2.3
ViM [71]	46.9±2.8	85.9±1.0	58.4±5.8	77.4±3.0	46.6±6.6	82.9±4.5	47.1±1.8	82.2±1.5	49.8±0.7	82.1±0.2
KNN [66]	57.0±5.1	81.8±3.2	58.7±5.9	80.7±2.8	51.9±3.7	84.0±1.3	47.4±5.6	83.0±1.7	53.7±0.4	82.4±0.2
VOS [16]	63.7±2.0	78.3±0.5	57.8±0.2	79.7±0.2	44.8±5.6	84.6±3.2	43.9±1.1	81.5±1.0	52.5±0.7	81.0±0.4
NPOS [67]	46.4±0.3	86.0±0.9	58.3±0.4	78.8±0.7	30.3±1.0	92.3±0.8	64.2±7.1	76.6±5.1	49.8±1.9	83.4±1.6
HOD ($\alpha = 0$)	34.1±2.5	89.0±1.6	36.6±2.4	84.6±1.0	28.5±2.2	90.5±0.2	14.9±1.0	93.7±0.2	28.5±0.4	89.4±0.5
HOD ($\alpha = 0.1$)	32.4±1.9	89.3±0.7	37.6±1.5	83.5±0.5	31.6±1.7	88.8±0.5	14.4±1.7	94.0±0.8	29.0±0.5	88.9±1.1

to capture certain types of variation, particularly the potentially problematic nature of locally parallel principal axes in learning hierarchical representations [9].

Low-dimensional out-of-distribution detection. Hyperbolic spaces leverage the representation space efficiently, enabling lower-dimensional embeddings for memory-constrained deployments, as shown in [38].

Table 4. OOD detection performance on ImageNet-200 as D_{id} . The values are the mean and standard deviation after training each method three times on ResNet-18. **Bold** if there is statistical significance difference.

Methods	D_{out}^{test}											
	SSB		Ninco		iNaturalist		Texture		OpenImage-O		Average	
	FPR95↓	AUROC↑	FPR95↓	AUROC↑	FPR95↓	AUROC↑	FPR95↓	AUROC↑	FPR95↓	AUROC↑	FPR95↓	AUROC↑
EBO [46]	70.0±0.4	79.7±0.1	50.7±0.9	85.1±0.1	26.3±2.3	92.5±0.5	41.3±1.9	90.8±0.2	37.2±1.7	89.1±0.3	45.1±14.7	87.4±4.6
ODIN [30]	74.9±0.2	76.9±0.1	60.1±0.9	83.3±0.1	22.4±1.8	94.4±0.4	43.0±1.4	90.7±0.2	37.7±1.0	90.0±0.2	47.6±18.2	87.1±6.2
MLS [28]	70.0±0.4	80.1±0.1	49.8±0.8	85.6±0.1	25.0±2.0	93.1±0.5	41.1±1.8	90.6±0.2	36.1±1.3	89.5±0.3	44.4±15.1	87.8±4.5
GradNorm [31]	83.6±0.9	71.3±0.5	83.0±0.3	73.3±0.7	61.4±3.0	86.1±2.0	66.8±3.5	86.1±0.4	71.6±0.4	80.4±1.2	73.3±8.8	79.4±6.2
ViM [71]	70.1±0.5	74.0±0.3	47.2±1.1	83.3±0.2	27.5±0.4	91.0±0.4	20.4±0.2	94.6±0.1	34.1±0.8	88.2±0.2	39.9±17.5	86.2±7.1
KNN [66]	72.3±0.5	77.0±0.2	46.7±0.8	86.1±0.1	24.4±1.0	94.0±0.4	24.5±0.2	95.3±0.02	33.4±1.3	90.1±0.3	40.3±18.0	88.5±6.6
VOS [16]	71.8±0.9	78.6±0.2	52.6±0.9	84.4±0.3	25.9±0.8	92.4±0.4	36.5±0.5	91.7±0.1	36.7±1.1	89.0±0.4	44.7±16.0	87.2±5.1
NPOS [67]	72.9±1.6	74.0±0.5	49.1±0.4	84.7±0.2	22.8±0.5	93.8±0.2	18.1±0.5	96.9±0.1	28.2±0.6	91.3±0.2	38.2±20.3	88.1±8.1
HOD ($\alpha = 0$)	66.2±1.9	75.5±0.5	44.5±2.1	85.4±0.2	19.8±0.5	93.7±0.3	28.3±1.7	92.6±0.3	0.0±0.0	100.0±0.0	31.8±22.4	89.4±8.4

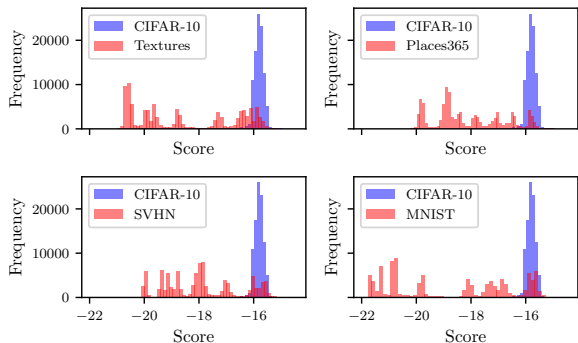


Figure 3. Histogram displaying scores for both ID and OOD datasets. Visualization reveals that distances to the in-distribution data are consistently lower than those to the out-of-distribution data.

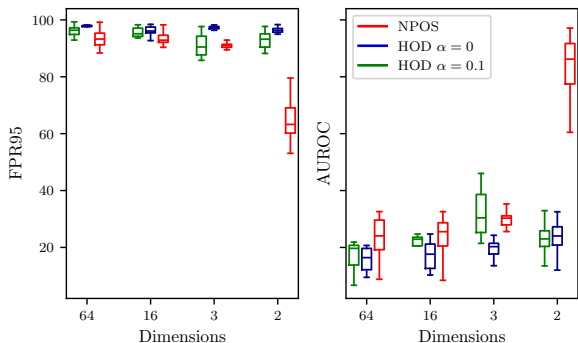


Figure 4. Boxplot illustrating OOD detection performance using CIFAR-10 as the ID dataset across three distinct training runs. We present FPR95 and AUROC metrics upon reducing the dimensionality of the ResNet-18 projection layer. The Hyperbolic space maintains robustness to dimensionality reduction for OOD detection, which offers a promising solution for limited resource devices.

We evaluate NPOS and HOD, with and without synthetic outlier sampling, using projection layer dimensions of

{64, 16, 3, 2}. Hyperbolic embeddings outperform NPOS in OOD detection at lower dimensions Fig. 4, making them a promising solution for resource-limited devices.

5. Related Work

Out-of-Distribution detection. Research on OOD detection has witnessed significant advancements since the overconfidence phenomenon was discovered by [58]. Primarily revolving around two overarching methodologies: *post-hoc* techniques and *regularization-based* approaches.

Post-hoc methods perform OOD detection within pre-trained models through the development of scoring functions, some score functions include confidence-based methods [4, 26, 45], energy-based scores [46] distance-based [15, 43, 54, 62, 64], gradient-based [22, 31], and Bayesian approaches [18, 21, 36, 39, 49, 72]. However, those methodologies are based on Euclidean models which struggle to capture intricate hierarchical structures often found in natural images. Some works suggested using the Hyperbolic space for OOD detection [23, 69], yet they have fallen short of achieving competitive results compared to the current state-of-the-art. HOD address this gap by proposing a methodology to train effective Hyperbolic networks.

On a different line, regularization-based approaches, which focus on training-time adjustments to the model to foster better discrimination between ID and OOD data [5, 20, 25, 32, 50, 51, 74]. These methods often involve regularization techniques aimed at encouraging the model to produce lower confidence [27, 42] or higher energy score [16, 33, 46, 53].

However, these methods require the availability of auxiliary OOD datasets. Notably, methods like VOS [16] and NPOS [67] have pioneered the synthesis of outliers, providing a flexible alternative to using real OOD data for model regularization. Despite these advancements, challenges persist, particularly to know the nature of the ID we are sampling from, without assuming any distributional assumption. Hence, we propose a new framework to sample the

synthetic outliers in the Hyperbolic space. Due to its hierarchical nature, we can sample from those ID embeddings that are more uncertain or encompass broader concepts aiming to alleviate such limitations and further refine the efficacy of OOD detection methodologies.

Hyperbolic representation. Hyperbolic space has gained significant attention in DL, particularly for tasks involving hierarchical structures, *i.e.*, tree-like structures and taxonomies [40, 59, 65], text representations [10, 14, 78], graphs [3, 8, 11]. Previous research has underscored the potential of adopting a hierarchical perspective for OOD detection. For instance, [17] uses the Hyperbolic space to provide an uncertainty score for time series. Similarly, the distance to the origin in the Poincaré ball has been highlighted to be a good uncertainty metric used for image segmentation [2], classification [35] and few-shot learning [1]. The use of softmax and energy score have been explored in the Hyperbolic space too [23, 69]. Yet they were not competitive with the Euclidean-based methodologies. Our work addresses the limitations encountered by previous approaches leveraging the Hyperbolic structure to learn a clear boundary between in-distribution and out-of-distribution data achieving state-of-the-art performance for OOD detection.

6. Limitations

While our study utilized ResNet-18 as the backbone due to its established performance, it's important to note that our analyses did not uncover the impact of Hyperbolic embeddings within architectures of varying depths. Furthermore, we did not investigate their effects beyond natural image datasets, such as in medical domains. Moving forward, we aim to address these limitations by exploring fully Hyperbolic architectures [44, 52] to leverage the hierarchical embeddings they offer. However, training such architectures can be complex and prone to numerical instability [55]. In the same line, computing exponential map and losses requires the use of FP64 precision to avoid any NaN values, which unfortunately reduces the speed of the training process.

7. Conclusions

Traditional OOD detection methods have limitations, often suffering from overconfidence or reliance on external datasets. The introduction of Hyperbolic geometry as an alternative to the Euclidean space offers promising avenues for addressing these challenges. We developed a more effective framework, HOD, for OOD detection by leveraging the hierarchical representation capabilities of Hyperbolic space.

Our empirical evaluations demonstrated substantial performance improvements, outperforming existing state-of-

the-art methods in terms of FPR95 in CIFAR-10 and CIFAR-100 datasets. Additionally, we introduced a novel strategy for synthesizing outliers in Hyperbolic space to avoid the need for auxiliary datasets. Additionally, we showed that the Hyperbolic space holds potential for real-world deployment, especially in resource-constrained environments.

The implications of our findings extend beyond OOD detection, offering opportunities for practical applications across various industrial domains. By bridging the gap between Euclidean and Hyperbolic space, our research paves the way for more robust and efficient DL models capable of handling unforeseen data distributions.

References

- [1] Tejas Anvekar and Dena Bazazian. GPr-Net: Geometric Prototypical Network for Point Cloud Few-Shot Learning. In *Proceedings of the IEEE/CVF Conference on Computer Vision and Pattern Recognition*, pages 4178–4187, 2023. 8
- [2] Mina Ghadimi Atigh, Julian Schoep, Erman Acar, Nanne van Noord, and Pascal Mettes. Hyperbolic image segmentation. In *CVPR*, pages 4443–4452, 2022. 2, 3, 5, 8
- [3] Gregor Bachmann, Gary Bécigneul, and Octavian Ganea. Constant Curvature Graph Convolutional Networks. In *ICML*, pages 486–496, 2020. 8
- [4] Abhijit Bendale and Terrance E. Boult. Towards open world recognition. In *IEEE Conference on Computer Vision and Pattern Recognition, CVPR 2015, Boston, MA, USA, June 7-12, 2015*, pages 1893–1902. IEEE Computer Society, 2015. 7
- [5] Petra Bevandić, Ivan Krešo, Marin Oršić, and Siniša Šegvić. Discriminative out-of-distribution detection for semantic segmentation, 2018. 1, 7
- [6] Julian Bitterwolf, Maximilian Mueller, and Matthias Hein. In or out? fixing imagenet out-of-distribution detection evaluation. In *ICML*, 2023. 4
- [7] Martin R. Bridson and André Haefliger. *Metric Spaces of Non-Positive Curvature*. Springer, 1999. 1
- [8] Ines Chami, Zhitao Ying, Christopher Ré, and Jure Leskovec. Hyperbolic Graph Convolutional Neural Networks. In *NeurIPS*, 2019. 8
- [9] Seunghyuk Cho, Juyong Lee, Jaesik Park, and Dongwoo Kim. A rotated hyperbolic wrapped normal distribution for hierarchical representation learning. In *NeurIPS*, 2022. 6
- [10] Mircea Cimpoi, Subhansu Maji, Iasonas Kokkinos, Sammy Mohamed, and Andrea Vedaldi. Describing textures in the wild. In *CVPR*, pages 3606–3613, 2014. 4, 8
- [11] Jindou Dai, Yuwei Wu, Zhi Gao, and Yunde Jia. A Hyperbolic-to-Hyperbolic Graph Convolutional Network. In *CVPR*, pages 154–163, 2021. 8
- [12] Jia Deng, Wei Dong, Richard Socher, Li-Jia Li, Kai Li, and Fei-Fei Li. Imagenet: A large-scale hierarchical image database. In *CVPR*, pages 248–255, 2009. 4
- [13] Li Deng. The MNIST database of handwritten digit images for machine learning research [best of the web]. *IEEE Signal Processing Magazine*, 29(6):141–142, 2012. 4

- [14] Karan Desai, Maximilian Nickel, Tanmay Rajpurohit, Justin Johnson, and Ramakrishna Vedantam. Hyperbolic image-text representations, 2023. [1](#), [2](#), [3](#), [8](#)
- [15] Xuefeng Du, Gabriel Gozum, Yifei Ming, and Yixuan Li. SIREN: Shaping representations for detecting out-of-distribution objects. In *Advances in Neural Information Processing Systems*, 2022. [7](#)
- [16] Xuefeng Du, Zhaoning Wang, Mu Cai, and Yixuan Li. VOS: learning what you don’t know by virtual outlier synthesis. In *ICLR*. OpenReview.net, 2022. [1](#), [4](#), [5](#), [6](#), [7](#)
- [17] Alessandro Flaborea, Bardh Prenkaj, Bharti Munjal, Marco Aurelio Sterpa, Dario Aragona, Luca Podo, and Fabio Galasso. Are we certain it’s anomalous? *CVPRW*, 2022. [8](#)
- [18] Yarin Gal and Zoubin Ghahramani. Dropout as a bayesian approximation: Representing model uncertainty in deep learning. In *ICML*, pages 1050–1059, 2016. [7](#)
- [19] Octavian-Eugen Ganea, Gary Bécigneul, and Thomas Hofmann. Hyperbolic entailment cones for learning hierarchical embeddings. In *ICML*, pages 1632–1641, 2018. [1](#)
- [20] Yonatan Geifman and Ran El-Yaniv. Selectivenet: A deep neural network with an integrated reject option. In *ICML*, pages 2151–2159, 2019. [1](#), [7](#)
- [21] Alvaro Gonzalez-Jimenez, Simone Lionetti, Philippe Gottfroid, Fabian Gröger, Marc Pouly, and Alexander A. Navarini. Robust T-Loss for Medical Image Segmentation. In *MICCAI*, pages 714–724, 2023. [7](#)
- [22] Alvaro Gonzalez-Jimenez, Simone Lionetti, Marc Pouly, and Alexander A. Navarini. SANO: Score-Based Diffusion Model for Anomaly Localization in Dermatology. In *CVPRW*, pages 2988–2994, 2023. [7](#)
- [23] Yunhui Guo, Xudong Wang, Yubei Chen, and Stella X. Yu. Clipped hyperbolic classifiers are super-hyperbolic classifiers. In *CVPR*, pages 1–10, 2022. [2](#), [5](#), [7](#), [8](#)
- [24] Kaiming He, Xiangyu Zhang, Shaoqing Ren, and Jian Sun. Deep residual learning for image recognition. In *CVPR*, pages 770–778, 2016. [5](#)
- [25] Matthias Hein, Maksym Andriushchenko, and Julian Bitterwolf. Why relu networks yield high-confidence predictions far away from the training data and how to mitigate the problem. In *CVPR*, pages 41–50, 2019. [1](#), [7](#)
- [26] Dan Hendrycks and Kevin Gimpel. A baseline for detecting misclassified and out-of-distribution examples in neural networks. In *ICLR*, 2017. [7](#)
- [27] Dan Hendrycks, Mantas Mazeika, and Thomas G. Dietterich. Deep anomaly detection with outlier exposure. In *ICLR*, 2019. [7](#)
- [28] Dan Hendrycks, Steven Basart, Mantas Mazeika, Andy Zou, Joseph Kwon, Mohammadreza Mostajabi, Jacob Steinhardt, and Dawn Song. Scaling out-of-distribution detection for real-world settings. In *ICML*, pages 8759–8773, 2022. [5](#), [6](#), [7](#)
- [29] Grant Van Horn, Oisín Mac Aodha, Yang Song, Yin Cui, Chen Sun, Alexander Shepard, Hartwig Adam, Pietro Perona, and Serge J. Belongie. The inaturalist species classification and detection dataset. In *CVPR*, pages 8769–8778, 2018. [4](#)
- [30] Yen-Chang Hsu, Yilin Shen, Hongxia Jin, and Zsolt Kira. Generalized ODIN: detecting out-of-distribution image without learning from out-of-distribution data. In *CVPR*, pages 10948–10957, 2020. [5](#), [6](#), [7](#)
- [31] Rui Huang, Andrew Geng, and Yixuan Li. On the importance of gradients for detecting distributional shifts in the wild. In *NeurIPS*, pages 677–689, 2021. [5](#), [6](#), [7](#)
- [32] Taewon Jeong and Heeyoung Kim. OOD-MAML: meta-learning for few-shot out-of-distribution detection and classification. In *NeurIPS*, 2020. [1](#), [7](#)
- [33] Julian Katz-Samuels, Julia B. Nakhleh, Robert D. Nowak, and Yixuan Li. Training OOD detectors in their natural habitats. In *ICML*, pages 10848–10865, 2022. [7](#)
- [34] Prannay Khosla, Piotr Teterwak, Chen Wang, Aaron Sarna, Yonglong Tian, Phillip Isola, Aaron Maschiot, Ce Liu, and Dilip Krishnan. Supervised Contrastive Learning. In *NeurIPS*, pages 18661–18673, 2020. [3](#)
- [35] Valentin Khrulkov, Leyla Mirvakhabova, Evgeniya Ustinova, Ivan V. Oseledets, and Victor S. Lempitsky. Hyperbolic image embeddings. In *CVPR*, pages 6417–6427, 2020. [1](#), [2](#), [3](#), [5](#), [8](#)
- [36] Agustinus Kristiadi, Matthias Hein, and Philipp Hennig. Being bayesian, even just a bit, fixes overconfidence in relu networks. In *ICML*, pages 5436–5446, 2020. [7](#)
- [37] Alex Krizhevsky. Learning multiple layers of features from tiny images, 2009. [4](#)
- [38] Aditya Kusupati, Gantavya Bhatt, Aniket Rege, Matthew Wallingford, Aditya Sinha, Vivek Ramanujan, William Howard-Snyder, Kaifeng Chen, Sham Kakade, Prateek Jain, and Ali Farhadi. Matryoshka representation learning. In *NeurIPS*, pages 30233–30249, 2022. [6](#)
- [39] Balaji Lakshminarayanan, Alexander Pritzel, and Charles Blundell. Simple and scalable predictive uncertainty estimation using deep ensembles. In *NeurIPS*, pages 6402–6413, 2017. [7](#)
- [40] Marc Law, Renjie Liao, Jake Snell, and Richard Zemel. Lorentzian Distance Learning for Hyperbolic Representations. In *ICML*, pages 3672–3681, 2019. [1](#), [2](#), [8](#)
- [41] John M. Lee. *Riemannian Manifolds*. Springer, New York, NY, 1997. [2](#)
- [42] Kimin Lee, Honglak Lee, Kibok Lee, and Jinwoo Shin. Training confidence-calibrated classifiers for detecting out-of-distribution samples. In *ICLR*, 2018. [7](#)
- [43] Kimin Lee, Kibok Lee, Honglak Lee, and Jinwoo Shin. A simple unified framework for detecting out-of-distribution samples and adversarial attacks. In *NeurIPS*, pages 7167–7177, 2018. [7](#)
- [44] Keegan Lensink, Bas Peters, and Eldad Haber. Fully Hyperbolic Convolutional Neural Networks for Computer Vision. In *ICLR*, 2023. [4](#), [8](#)
- [45] Shiyu Liang, Yixuan Li, and R. Srikant. Enhancing the reliability of out-of-distribution image detection in neural networks. In *ICLR*, 2018. [7](#)
- [46] Weitang Liu, Xiaoyun Wang, John D. Owens, and Yixuan Li. Energy-based out-of-distribution detection. In *NeurIPS*, 2020. [5](#), [6](#), [7](#)

- [47] I. Loshchilov and F. Hutter. Sgdr: Stochastic gradient descent with warm restarts. *ICLR*, 2016. 5
- [48] Ilya Loshchilov and Frank Hutter. Decoupled weight decay regularization. In *ICLR*, 2019. 5
- [49] Wesley J. Maddox, Pavel Izmailov, Timur Garipov, Dmitry P. Vetrov, and Andrew Gordon Wilson. A simple baseline for bayesian uncertainty in deep learning. In *NeurIPS*, pages 13132–13143, 2019. 7
- [50] Andrey Malinin and Mark J. F. Gales. Predictive uncertainty estimation via prior networks. In *NeurIPS*, pages 7047–7058, 2018. 1, 7
- [51] Alexander Meinke and Matthias Hein. Towards neural networks that provably know when they don’t know. In *ICLR*, 2020. 1, 7
- [52] Pascal Mettes, Mina Ghadimi Atigh, Martin Keller-Ressel, Jeffrey Gu, and Serena Yeung. Hyperbolic deep learning in computer vision: A survey, 2023. 2, 8
- [53] Yifei Ming, Ying Fan, and Yixuan Li. POEM: out-of-distribution detection with posterior sampling. In *ICML*, pages 15650–15665, 2022. 7
- [54] Yifei Ming, Yiyou Sun, Ousmane Dia, and Yixuan Li. How to exploit hyperspherical embeddings for out-of-distribution detection? In *ICLR*, 2023. 1, 7
- [55] Gal Mishne, Zhengchao Wan, Yusu Wang, and Sheng Yang. The Numerical Stability of Hyperbolic Representation Learning. In *ICML*, pages 24925–24949, 2023. 2, 8
- [56] Yoshihiro Nagano, Shoichiro Yamaguchi, Yasuhiro Fujita, and Masanori Koyama. A Wrapped Normal Distribution on Hyperbolic Space for Gradient-Based Learning. In *ICML*, pages 4693–4702, 2019. 4
- [57] Yuval Netzer, Tao Wang, Adam Coates, Alessandro Bisacco, Bo Wu, and Andrew Ng. Reading digits in natural images with unsupervised feature learning. In *NeurIPS*, 2011. 4
- [58] Anh Mai Nguyen, Jason Yosinski, and Jeff Clune. Deep neural networks are easily fooled: High confidence predictions for unrecognizable images. In *CVPR*, pages 427–436, 2015. 1, 7
- [59] Maximilian Nickel and Douwe Kiela. Poincaré embeddings for learning hierarchical representations. In *NeurIPS*, 2017. 2, 8
- [60] Jiwoong Park, Junho Cho, Hyung Jin Chang, and Jin Young Choi. Unsupervised hyperbolic representation learning via message passing auto-encoders. In *CVPR*, pages 5516–5526, 2021. 1
- [61] Wei Peng, Tuomas Varanka, Abdelrahman Mostafa, Henglin Shi, and Guoying Zhao. Hyperbolic deep neural networks: A survey, 2021. 1
- [62] Jie Ren, Stanislav Fort, Jeremiah Liu, Abhijit Guha Roy, Shreyas Padhy, and Balaji Lakshminarayanan. A simple fix to mahalanobis distance for improving near-OOD detection. *ArXiv preprint*, abs/2106.09022, 2021. 7
- [63] Frederic Sala, Christopher De Sa, Albert Gu, and Christopher Ré. Representation tradeoffs for hyperbolic embeddings. In *ICML*, pages 4457–4466, 2018. 1
- [64] Vikash Sehwal, Mung Chiang, and Prateek Mittal. SSD: A unified framework for self-supervised outlier detection. In *ICLR*, 2021. 7
- [65] Ryohei Shimizu, Yusuke Mukuta, and Tatsuya Harada. Hyperbolic neural networks++. In *ICLR*, 2021. 1, 8
- [66] Yiyou Sun, Yifei Ming, Xiaojin Zhu, and Yixuan Li. Out-of-distribution detection with deep nearest neighbors. In *ICML*, pages 20827–20840, 2022. 1, 5, 6, 7
- [67] Leitian Tao, Xuefeng Du, Jerry Zhu, and Yixuan Li. Non-parametric outlier synthesis. In *ICLR*, 2022. 1, 4, 5, 6, 7
- [68] Alexandru Tifrea, Gary Bécigneul, and Octavian-Eugen Ganea. Poincaré GloVe: Hyperbolic Word Embeddings, 2018. 2
- [69] Max van Spengler, E. Berkhout, and P. Mettes. Poincaré resnet. *ICCV*, 2023. 2, 5, 7, 8
- [70] Sagar Vaze, Kai Han, Andrea Vedaldi, and Andrew Zisserman. Open-set recognition: A good closed-set classifier is all you need. In *ICLR*, 2022. 4
- [71] Haoqi Wang, Zhizhong Li, Litong Feng, and Wayne Zhang. ViM: Out-of-distribution with virtual-logit matching. In *CVPR*, 2022. 4, 5, 6, 7
- [72] Yeming Wen, Dustin Tran, and Jimmy Ba. Batchensemble: an alternative approach to efficient ensemble and lifelong learning. In *ICLR*, 2020. 7
- [73] Pingmei Xu, Krista A Ehinger, Yinda Zhang, Adam Finkelstein, Sanjeev R. Kulkarni, and Jianxiong Xiao. Turkergaze: Crowdsourcing saliency with webcam based eye tracking. *arXiv preprint arXiv: 1504.06755*, 2015. 4
- [74] Jingyang Zhang, Haoqi Wang, Litong Feng, Xiaopeng Yan, Huabin Zheng, Wayne Zhang, and Ziwei Liu. Semantically coherent out-of-distribution detection. In *ICCV*, pages 8281–8289, 2021. 1, 7
- [75] Fisher Yu, Ari Seff, Yinda Zhang, Shuran Song, Thomas Funkhouser, and Jianxiong Xiao. Lsun: Construction of a large-scale image dataset using deep learning with humans in the loop, 2015. 4
- [76] Jingyang Zhang, Jingyang Yang, Pengyun Wang, Haoqi Wang, Yueqian Lin, Haoran Zhang, Yiyou Sun, Xuefeng Du, Kaiyang Zhou, Wayne Zhang, Yixuan Li, Ziwei Liu, Yiran Chen, and Hai Li. OpenOOD v1.5: Enhanced benchmark for out-of-distribution detection, 2023. 4, 5
- [77] Bolei Zhou, Agata Lapedriza, Aditya Khosla, Aude Oliva, and Antonio Torralba. Places: A 10 million image database for scene recognition. *IEEE TPAMI*, 40(6):1452–1464, 2017. 4
- [78] Yudong Zhu, Di Zhou, Jinghui Xiao, Xin Jiang, Xiao Chen, and Qun Liu. HyperText: Endowing FastText with Hyperbolic Geometry. In *Findings of the Association for Computational Linguistics : EMNLP 2020*, pages 1166–1171, Online, 2020. Association for Computational Linguistics. 8